A collagen-conducting polymer composite with enhanced chondrogenic potential

CP-Collagen Composite with Chondrogenic Potential

Rebecca L. Keate[1, 2, 3], Joshua Tropp[1, 2, 3], Carlos Serna III[4], Jonathan Rivnay[1, 2, 3]

[1]Department of Biomedical Engineering, [2]Center for Advanced Regenerative Engineering, [3]Simpson Querrey Institute, Northwestern University, [4]Feinberg School of Medicine, Division of Plastic Surgery

Evanston, Illinois 60208, United States

Correspondence: Jonathan Rivnay

Phone: 847 467 6622

Email: jrivnay@northwestern.edu

Abstract

Introduction Conducting polymers (CPs) have demonstrated promise for promoting tissue repair, yet their ability to facilitate cartilage regeneration has yet to be thoroughly investigated. Integrating CPs into common scaffolds for tissue regeneration, such as collagen, would enable mechanistic studies on the potential for CPs to promote cartilage repair. Here, we combine absorbable collagen sponges (ACS) with the CP PEDOT-S and show that the PEDOT-S-collagen composite (PEDOT-ACS) has enhanced chondrogenic potential compared to the collagen sponge alone.

Methods PEDOT-S was incorporated through a simple incubation process. Changes to scaffold topography, elastic modulus, swelling ratio, and surface charge were measured to analyze how PEDOT-S affected the material properties of the scaffold. Changes in rat bone marrow mesenchymal stem cell (rBMSC) functionality were assessed with cell viability and glycosaminoglycan production assays.

Results Macrostructure and microstructure of the scaffold remained largely unaffected by PEDOT-S modification, as observed through SEM images and quantification of scaffold porosity. Zeta potential, swelling ratio, and dry elastic modulus of the collagen scaffold were significantly changed by the incorporation of PEDOT-S. Cells seeded on PEDOT-ACS improved cell viability and enhanced glycosaminoglycan production.

Conclusion We demonstrate a practical approach to generate PEDOT-S composites with comparable physical properties to pristine collagen scaffolds. We show that PEDOT-ACS can influence cell functionality and serve as a promising model system for mechanistic investigations on the roles of bioelectronic signaling in the repair of cartilage and other tissue types.

Keywords: PEDOT, bioelectronics, chondrocyte differentiation, cartilage engineering

Brief Biography *(per special instruction for 2021 Young Innovators Special Issue)*

Jonathan earned his B.Sc. in 2006 from Cornell University (Ithaca, NY). He then moved to Stanford University (Stanford, CA) where he earned a M.Sc. and Ph.D. in Materials Science and Engineering studying the structure and electronic transport properties of organic electronic materials. In 2012, he joined the Department of Bioelectronics at the Ecole des Mines de Saint-Etienne in France as a Marie Curie post-doctoral fellow, working on conducting polymer-based devices for bioelectronics. Jonathan spent 2015-2016 as a member of the research staff in the Printed Electronics group at the Palo Alto Research Center (Palo Alto, CA) before joining the Department of Biomedical Engineering at Northwestern University in 2017. He is a recipient of an NSF CAREER award, ONR Young Investigator award, and has been named an Alfred P. Sloan Research Fellow, and MRS Outstanding Early Career Investigator.

Abbreviations, symbols, and terminology:

ACS – absorbable collagen sponges

PEDOT-S - Poly(4-(2,3-dihydro-thieno[3,4-*b*][1,4]dioxin-2-ylmethoxy)-butane-1-sulfonic acid sodium salt

PEDOT-ACS - Poly(4-(2,3-dihydro-thieno[3,4-*b*][1,4]dioxin-2-ylmethoxy)-butane-1-sulfonic acid sodium salt-absorbable collagen sponge composite

CP – conducting polymer

Introduction

Electrical signaling and stimulation can be a powerful tool for directing maintenance and repair of various tissue systems.[1-3] To leverage the benefits of these signaling regimes, electroactive materials are increasingly investigated for their potential to facilitate regeneration. Conducting polymers (CPs), in particular, have been documented as beneficial and diverse tools in improving regenerative outcomes. CPs have demonstrated the capabilities to direct cellular phenomena, such as adhesion,[4,5] migration,[6-8] and differentiation,[9-11] and have shown potential for improving tissue regenerative outcomes in numerous tissue types including skin, nerve, and bone.[12-15]

The use of CPs for supporting cartilage repair has also recently been demonstrated, although such investigations remain rare.[16,17] Cartilage engineering is important for various musculoskeletal disorders[18], with osteoarthritis being among the most common. Osteoarthritis is a highly prevalent degenerative joint disease in which cartilage degradation leads to limited mobility and joint pain.[19] Over 20% of adults develop osteoarthritis, yet it has no cure.[20] A major complication in treating osteoarthritis and other cartilage-related injuries is the tissue's limited capability for intrinsic repair.[21] While the electromechanical properties of cartilage are well-documented, the potential for CPs and their associated bioelectronic devices to facilitate cartilage regeneration remains unclear.[22,23] Using CPs to investigate the mechanisms by which electrical signaling promotes cartilage repair thus presents an opportunity to identify more effective therapeutic strategies, yet there is no existing platform well-suited to perform comprehensive studies on the role of electrical signaling in regenerative engineering.

Combining CPs with natural polymers offers an opportunity to generate a biomimetic composite system that can act as both an engineered bioelectronic regenerative platform, as well as a tool for understanding the role of electroactive materials and bioelectricity in regeneration.[24] If these materials are to act as a representative model for understanding the physiological role of electrical signals in

driving tissue regeneration, the scaffold should be comprised of components that mimic the native cell environment. ECM-based scaffolds, including those based on collagen, have shown promise for cartilage tissue engineering applications for their ability to promote cell adhesion and other desirable cellular functionalities.[25,26] Despite these benefits, some limitations of current collagenous materials in cartilage engineering applications include its poor mechanical strength and inability to enhance chondrogenic outcomes, which potentially may be bolstered by augmenting collagen with electroactive properties. Absorbable collagen sponges (ACS) are commercially available 3D macroporous scaffolds comprised of type I collagen. Previous studies have demonstrated that such scaffolds are a useful platform to investigate novel cartilage regenerative strategies, such as molecular enhancements,[27] cell therapies,[28] or structural augmentations[29] that may promote tissue repair.

The conducting polymer poly(3,4-ethylenedioxythiophene) (PEDOT), often complexed with the dopant polystyrene sulfonate (PSS), is among the most widely explored CPs for tissue engineering applications and have been shown to improve functional outcomes in diverse tissue types.[11,30,31] PEDOT:PSS owes its popularity to its biocompatibility and commercial availability, which makes it accessible for biomedical applications. A major drawback to aqueous dispersions of PEDOT, such as PEDOT:PSS, is the requirement of various low molecular weight additives,[32] often ill characterized, which may limit its range of usable concentrations, and complicate coating uniformity, functionalization, and characterization.[33,34]

One approach to mitigate these complications is to use a derivative of PEDOT which can be chemically modified to promote water solubility.[33] Poly(4-(2,3-dihydro-thieno[3,4-*b*][1,4]dioxin-2-ylmethoxy)-butane-1-sulfonic acid sodium salt (PEDOT-S) **(Figure 1a)** is an easily accessible self-doped PEDOT derivative that offers a more versatile solution to interface with biological materials.[35,36] PEDOT-S also offers as a platform for further synthetic modification that may grant the molecule enhanced capabilities to influence cell functionality.

In this study, we demonstrate a facile approach to generate a CP-collagen composite using an absorbable collagen sponge (ACS) and PEDOT-S. We demonstrate that PEDOT-S incorporation into collagen scaffolds yields a composite that is structurally comparable to pristine collagen and bolsters rat bone marrow mesenchymal stem cell (rBMSC) viability. Additionally, we show preliminary evidence that the PEDOT-S-ACS composites (PEDOT-ACS) drive rBMSCs toward chondrocyte differentiation by analyzing glycosaminoglycan (GAG) production. The investigation presented here indicates that CP-collagen composites can enhance chondrogenic differentiation compared to their inert counterparts. Up to this point, studies exploring the role of CPs for cartilage engineering have been scarce, and to the authors' knowledge, no present study has explored the chondrogenic potential of PEDOT or its derivatives. Here, we lay the foundations for biomimetic, tissue-integrated CP bioelectronics and their potential to improve outcomes in cartilage engineering applications.

Methods

Polymer Synthesis

Iron (III) chloride ($FeCl_3$) was purchased from ThermoFisher Scientific (Ward Hill, MA). Sodium persulfate ($Na_2S_2O_8$) was purchased from Acros Organics (Fair Lawn, NJ). All other chemicals were reagent grade and used as received. 4-(2,3-Dihydro-thieno[3,4-*b*][1,4]dioxin-2-ylmethoxy)-butane-1-sulfonic acid sodium salt (EDOT-S) was synthesized as previously described.[37] PEDOT-S was synthesized via chemical oxidative polymerization using $FeCl_3$ as a catalyst and $Na_2S_2O_8$ as a primary oxidant according to previously published methods.[36] This method is widely reported for PEDOT-S and similar conjugated homopolymers because of its simplicity and low cost.[38]

Composite Formation

Sheets of absorbable collagen sponges (ACS) (Helistat; Integra Life Sciences, Plainsboro, NJ) were cut into individual scaffolds (5mm $\times$ 5mm $\times$ 5mm). Polymer solutions were prepared by dissolving PEDOT-S

(20 mg mL^{-1}) in Dulbecco's phosphate buffered saline (DPBS) and shaking overnight. After the PEDOT-S was solubilized, 10 v/v% 1.24 M ammonium persulfate (APS) (Sigma; St. Louis, MO) was added to the PEDOT-S solution to ensure the molecule was fully doped.

The PEDOT-S solution was pre-incubated at 37 °C for 10 minutes prior to adding the sponges. ACS was incubated at a density of 5 scaffolds/1 mL of PEDOT-S solution for 30 minutes. After incubation, the sponges were rinsed in deionized (DI) H_2O and soaked in DPBS overnight to allow any excess PEDOT-S to leech out from the sponge. PEDOT-S-collagen composites (PEDOT-ACS) were then rinsed in DI H_2O, frozen in DI H_2O at -80 °C, and lyophilized overnight. After incubation in PEDOT-S, the ACS demonstrated a visible color change, attributable to the presence of PEDOT-S and indicative of polymer incorporation within the collagen matrix **(Figure 1b-c)**.

Scanning Electron Microscopy

All samples were directly mounted onto pin stubs with carbon tape prior to imaging and then sputter coated with 5 nm of gold/palladium with a Denton Desk IV Sputter Coater prior to imaging. PEDOT-ACS and ACS samples were imaged by scanning electron microscopy (SEM, Hitachi 4800-S) using an accelerating voltage of 5 kV. Images were captured with Hitachi S-4800 PC-SEM software.

Confocal Microscopy

The imaging of collagen scaffolds was performed on a Nikon A1 laser scanning confocal microscope with a 10x objective lens. Nikon Elements software was used to capture images. Because collagen is auto fluorescent, no exogenous dyes or visualization agents were necessary and scaffolds could be imaged as is.[39] The scaffold fluorescence was recorded in the same channel as DAPI fluorescent stain, using a 405 laser. ACS exhibits a high degree of planar heterogeneity, and thus z-stacks were taken to capture representative depictions of the cell morphology and autofluorescence throughout the scaffold depth.

Z-stacks were taken in randomly selected regions with depths greater about 400 µm. ImageJ was used to generate 3-D projections of the z-stacks.

Swelling

Samples were weighed before hydration and placed in DPBS at room temperature for 2 days. The samples were lightly blotted on a petri dish to remove excess water and weighed once more. Swelling ratio was calculated as the mass of the hydrated scaffold to that of the dry scaffold using the following:

$$swelling\ ratio = \frac{m_f - m_i}{m_i} * 100$$

Porosity and Pore Size

The porous percentage of the scaffolds was determined according to the method originally described by Ma et al.[40,41] Briefly, initial weight of scaffolds were measured, and they were then soaked in ethanol at room temperature for 24 hours. The final mass of the scaffolds after the ethanol soak was recorded and porosity was calculated according to the following equation[41]:

$$porosity\ (\%) = \frac{(W_f - W_0)\rho_1}{\rho_1 W_f + (\rho_2 - \rho_1)W_0} * 100$$

where ρ_1 represents the density of collagen, 1.21 g/mL, and ρ_2 represents the density of ethanol, 0.79 g/mL.

Pore size was quantified from SEM images. Two images were taken per scaffold and three different scaffolds were imaged per condition. An open source MATLAB code was then used to quantify pore radius as previously described.[42,43]

Mechanical Testing

For mechanical testing, ACS and PEDOT-ACS scaffolds (n=5) were punched into 10-mm discs with a biopsy punch. Compressive tests were performed with a Dynamic Mechanical Analyzer (DMA) (RSA-G2 Solids Analyzer, TA Instruments). Samples were tested at a constant linear strain rate of 2 mm/min at room temperature.[44] The elastic modulus of the samples was calculated from the linear portion of the stress-strain curves. ACS and PEDOT-ACS composites were tested under both dry and wet conditions. For the wet conditions, samples were incubated in DPBS at room temperature for one week and excess liquid was then removed from the surface of the sample before testing by blotting on a petri dish.

Zeta Potential

Approximately 10 mg of each scaffold variant was swollen in DI H_2O to equilibrium state and then frozen in liquid nitrogen. The samples were then pulverized into smaller particles using a pestle and resuspended in 5 mL of a 0.01 M NaCl electrolyte solution. The pH of the suspension solution was adjusted to 7.4 using 0.01 M NaOH. The ground particulates were then filtered using a 70 μm strainer (Corning CLS431751, Corning, NY) and loaded into a Malvern DTS1070 capillary cell (Malvern, United Kingdom). The zeta potential was measured on a Malvern Zetasizer NanoZSP (Malvern, United Kingdom) applying the Smoluchowski equation for large particles.[45,46] Measurements were taken in triplicates for each suspension of sponge particles and all results met quality criteria.

Cell Viability

Rat bone marrow mesenchymal stem cells (rBMSCs) from Cell Biologics were cultured according to the manufacturer's instructions. Briefly, cells were cultured in low glucose DMEM (Lonza 12-707F) supplemented with 10% FBS (GenDepot F0600-050), 1% Glutamax (Gibco 35050-061), and 1% antibiotic-antimycotic (GenDepot CA002-010). About 150,000 cells were seeded per scaffold.

An alamarBlue cell viability assay (ThermoFisher DAL1025) was performed according to the manufacturer's instructions to screen the composites for cytotoxic effects. Cells were incubated in cell

media containing 10% alamarBlue solution for 4 hours. Absorption of the solution was measured at 570 nm and 600 nm in a 96-well plate, separate from the scaffolds. The 600 nm reading acts as a measure of background noise, and this is used to normalize the 570 nm reading. The assay was also performed on PEDOT-ACS and ACS scaffolds without cells to ensure that scaffold background absorption would not confound viability results. Measurements were taken on day 0, 1, 2, 3, 5, and 7, where day 0 was the day of cell seeding. Cell viability percentages were calculated by normalizing the absorbance readings of the experimental scaffolds to pristine ACS.

Live/dead staining (Invitrogen L3224) was performed 72 hours after cell seeding to qualitatively examine the effects of the scaffold on cell viability and morphology. Imaging was performed on a Nikon C2+ scanning confocal microscope and images were captured with Nikon Elements Software. ImageJ was used to generate 3-D projections of the z-stacks.

Dimethylmethylene Blue Assay

The rBMSCs were cultured in chondrogenic media (ThermoFisher) for 14 days. Papain buffer was prepared with final concentrations of 5 mM l-cysteine (Sigma; St. Louis, MO), 0.1 mM EDTA (Sigma; St. Louis, MO), and 5 U/mL of papain (Sigma; St. Louis, MO). Samples were then digested in the papain buffer overnight at 75 °C. A DMMB assay was performed to quantify sulfonated glycosaminoglycan (GAG) production. Dimethylmethylene blue (DMMB) solution was prepared with 3.04 g glycine, 1.6 g NaCl, 95 mL of 0.1 M acetic acid, and 16 mg of 1,9-dimethylmethylene blue (Sigma, St. Louis, MO).[47] Samples were measured in a 96-well plate at 525 and 595 nm, where each well contained 180 µL of DMMB solution and 20 µL of sample. The absorbance at 595 nm was subtracted from the absorbance at 525 nm to increase assay sensitivity.[48] Measurements were calibrated using chondroitin sulfate salt from bovine trachea (Sigma, St. Louis, MO). Blank samples were analyzed to ensure that the scaffold itself did not cause measurement noise.

The GAG measurements were normalized to DNA quantity. DNA content of the samples digested in papain buffer was measured using a Quant-iT PicoGreen dsDNA Reagent (ThermoFisher) according to the manufacturer's instructions.

Statistical Analysis

A two-tailed t-test was performed between all data comparing ACS and PEDOT-ACS, assuming equal variances in the samples analyzed. T-test was the statistical method of choice because the effects of only a single parameter, the presence or absence of PEDOT, were within the scope of this investigation. A 95% confidence interval was assumed, where $p<0.05$ is considered significant. All results are reported as the mean ± standard deviation.

Results

PEDOT-ACS Maintains Collagen Macrostructure

We sought to analyze whether the PEDOT-S incorporation compromised the structure of collagen or the overall properties of the material. To determine this, the sponge was first qualitatively examined using confocal microscopy. Composites derived from ACS demonstrate autofluorescence, due to the resonant structure of collagen, and this phenomena was leveraged to demonstrate maintenance of autofluorescence, and thus triple-helical collagen structure in PEDOT-ACS.[39] The structure of PEDOT-ACS could be visualized under confocal microscopy without additional dyes or other imaging agents **(Figure 2a-b)**. This result indicates that the PEDOT-S does not damage collagen's native crystalline triple helix structure responsible for the macromolecule's autofluorescence.[39] Although, the autofluorescence was visibly diminished in PEDOT-ACS compared to the ACS alone. It is possible that a small spectral overlap between the primary absorbance of PEDOT-S (400 – 800 nm),[36,49] and the emission of type I collagen (300 – 500 nm),[50-52] may lead to the observed diminishment in autofluorescence through the inner filter effect, a well-known phenomenon when working with CPs.[53]

In addition to confocal microscopy, SEM was performed to examine the macro and microstructure of the scaffolds. Qualitative examination of the images taken indicate that the macrostructure of the sponge was maintained between the ACS and PEDOT-ACS conditions **(Figure 2c-d)**. In both sponges, pores are visible and surrounded by sheet-like structures throughout the sponge. Upon closer examination of the scaffolds, fibrous structures were apparent throughout both the ACS and PEDOT-ACS scaffolds **(Figure 2e-f)**. Differences in microstructure were more closely analyzed by quantifying differences in porous volume **(Figure 2g)** and pore size distribution **(Figure 2h)**. The porous volume of the ACS scaffold was found to be about less than 1% greater than the scaffold modified with PEDOT-S. While this difference was statistically significant, the low magnitude of the change in porosity indicates that the porous volume of the PEDOT-ACS remains comparable to the ACS alone. Changes to scaffold porosity were more closely analyzed by quantifying changes to pore size. Average pore size insignificantly changed in the CP scaffolds, where average pore radius for ACS and PEDOT-ACS scaffolds was about 7.3 ± 2.0 μm and 8.2 ± 1.9, respectively. The similarity in these averages is accompanied by pore size distributions that follow comparable trends between the modified and unmodified collagenous materials. Furthermore, the PEDOT-ACS scaffold microstructure remains largely comparable to that of the ACS alone following PEDOT-S incorporation.

Effect of PEDOT-S on Physical Properties of Collagen

Mechanical testing was performed to evaluate whether the PEDOT-S significantly compromised the structural integrity of the ACS (n=5). Under dry conditions, the average elastic modulus of ACS was about 7.15 ± 1.70 kPa, and the average elastic modulus of PEDOT-ACS was about 16.40 ± 4.08 kPa (p=0.001) **(Figure 3a).** Similarly, scaffolds were tested when wet, which more closely mimics the cellular environment. The average elastic modulus of the ACS when tested wet was about 0.518 ± 0.161 kPa and the elastic modulus of the PEDOT-ACS was about 0.529 ± 0.020 kPa (p=0.88) **(Figure 3b)**. Although the

PEDOT-ACS had a significantly higher modulus when tested dry, there is no significant difference between the ACS and PEDOT-ACS when evaluated under wet conditions.

In addition to the mechanical property evaluations, the swelling ratio of the scaffolds was also measured. The swelling ratio of the ACS alone was 361.5 ± 25.0 whereas the PEDOT-ACS swelling ratio was 337.7 ± 14.6 (p=0.02) **(Figure 3c)**. This reduction was statistically significant, yet the change is only about 6%. Taken together, these results indicate that the overall mechanical and swelling properties of the collagen scaffold is maintained even when PEDOT-S is incorporated.

PEDOT-S Influences Material Surface Charge

Zeta potential measurements were conducted to examine differences in surface charge attributable to the addition of PEDOT-S. The differences in bulk conductivity of the material are not expected to be measurable, considering the heterogeneous structure of the sponge and the limited percolation of the PEDOT-S throughout the scaffold. The zeta potential of ACS particles was -9.9 ± 1.3 mV, while the zeta potential of the PEDOT-ACS particles was about -19.9 ± 1.2 mV (p=0.0005) **(Figure 4).** This decrease in zeta potential can be attributed to the presence of the negatively charged sulfonates tethered to, but not compensating electron holes, on the PEDOT backbone. This result indicates that the approach used here effectively altered the surface charge of the collagen scaffold.

PEDOT-ACS Improves Cell Viability

Live/dead staining was performed to qualitatively examine cell morphology and identify potential cytotoxic effects of the scaffolds. Images were captured 72 hours after MSC seeding, revealing that cells on the PEDOT-S scaffolds exhibited a more elongated morphology than on the ACS scaffolds. Additionally, cell density appeared higher and fewer dead cells were observed on the PEDOT-ACS than on the ACS **(Figure 5a-b).**

Besides the qualitative examination, the cell health was quantified with an alamarBlue assay. On each day measurements were taken (0, 1, 2, 3, 5, 7), the cells on the PEDOT-ACS demonstrated higher viability than the cells on the collagen-only scaffolds (p=0.02, 0.11, 0.001, 0.006, 0.08, and 0.012) **(Figure 5c)**. The results of the qualitative live/dead imaging and the quantitative alamarBlue assay emphasizes that the incorporation of PEDOT-S is not cytotoxic, and that these scaffolds promote more ideal cell morphology and measurably higher cell viability than the ACS alone.

Chondrogenic Potential of PEDOT-ACS

A DMMB assay was performed to quantify cell GAG production and screen whether the PEDOT-ACS scaffolds may promote chondrocyte differentiation. After normalizing for the total DNA content of the sample, cells seeded on the PEDOT-ACS demonstrated an increase in GAG production over 140% **(Figure 6)**. Normalized GAG production for PEDOT-ACS was (1.1 ± 0.2) whereas for ACS was (0.4 ± 0.2) (p=0.01). This result demonstrates that not only do the PEDOT-ACS scaffolds support cell viability more than their inert counterparts, but they also have the capability to influence cell functionality. The observed increase in GAG production also indicates that these scaffolds may have promise for facilitating cartilage engineering and also investigating the mechanisms of electrical signaling on cartilage repair.

Discussion

In this study, we propose a straight-forward approach for developing electroactive composites through the incorporation of a water-soluble CP into ACS. Traditional approaches for incorporating CPs into natural biomaterials are challenging, generally requiring arduous multi-step procedures, potentially toxic additives and reagents, and pose a barrier to accessing conducting biocomposites.[24] The single component water-soluble CP PEDOT-S has been demonstrated here as efficacious for incorporating CP components into a collagen scaffold. Using this polymer in the material modification protocol offers more systematic control over CP concentrations than is possible with dilute aqueous dispersions such as

PEDOT:PSS. This method may be important for facilitating future investigations on the role of bioelectric signaling in tissue repair.

Material properties of the scaffold were examined to determine whether this incorporation protocol sacrificed any of the biologically favorable properties of collagen. SEM and confocal microscopy qualitatively showed PEDOT-S addition maintained the bulk collagen macrostructure. Higher magnification SEM images revealed a maintenance of fibrous structures throughout both the ACS and PEDOT-ACS scaffolds. Analysis of porous volume and pore size distribution revealed the overall structure of the collagen remained comparable after PEDOT-S was incorporated into the scaffolds. This further emphasizes that this method of conductive polymer functionalization offers a promising opportunity to augment the electrical properties of collagenous materials.

The influence of PEDOT-S on the overall architecture of collagen fibers may require further investigation and could be attributed to several different factors. Previous work has demonstrated that collagen fibrillogenesis is influenced by electrostatic interactions.[54] For example, it is possible that PEDOT-S alters the electrostatic interactions of the collagen and drives fibril rearrangement. Hamedi et al. previously demonstrated that amyloid protein structures can act as a template for PEDOT-S binding and the formation of nanofibrillar networks.[55,56] Xiao et al. similarly observed the formation of such fibrous structures when galvanostatically depositing PEDOT and collagen together.[57] The observation that CP integration affects collagen fibrillar structures is thus supported by existing literature. Despite this, further investigation is necessary to differentiate whether specific structures observed throughout the modified scaffold are PEDOT-S itself, PEDOT-S templated onto the existing collagen, or fibrillar collagen rearrangement due to changes in the local electrostatics. Since collagen is a major constituent of the extracellular matrix (ECM), it is highly relevant to understand the relationship between this protein structure and the electrical signaling that regulates homeostasis and repair.[3,58] This system presented

here offers a model to study the fundamental influence of physiological electroactive signaling on the structure of cell environments.

Compression testing was performed to determine whether the PEDOT-S influenced the bulk mechanical properties of the collagen structure. These experiments revealed that when wet, the PEDOT-ACS had a comparable modulus to ACS. Previous literature similarly demonstrates a decrease in swelling ratio and an increase in dry elastic modulus when PEDOT is incorporated into natural composites.[59-61] When incorporated into the natural biopolymer system, unlike prior examples with neutral PEDOT, [61] PEDOT-ACS showed a recovery of the elastic modulus when hydrated. This can be attributed to the hygroscopic nature of anionic PEDOT-S; a phenomenon readily observed in conjugated polyelectrolytes. This result is highly relevant to the ability of PEDOT-ACS composites to act as a future model system for investigating the interactions between cells and the bioelectronic signals that govern their behavior, since the PEDOT-S increases the material electroactivity without changing the material mechanics.

By quantifying cell health with an alamarBlue assay, we showed that the PEDOT-S incorporation was not cytotoxic. Cell health was significantly higher on PEDOT-ACS scaffolds than on ACS alone at several time points assessed. Live/dead staining showed rBMSCs had an elongated morphology on the scaffolds with PEDOT-S, indicating that the conductive polymer composite retained collagen's ability to facilitate direct cell attachment.[25,26] This agrees with other previous works that have demonstrated CPs can be used to tune and improve cell viability and adhesion.[61] This is potentially attributed to the mixed ionic/electronic conduction mechanisms that make CPs unique compared to other traditional inorganic electronic materials.[12] Future investigation between substrate oxidative state and/or conductivity and cell adhesion may be an interesting pursuit for this composite system to elucidate the cellular mechanisms by which bioelectronic signals can tune tissue functionality.

Lastly, we demonstrated that the PEDOT-ACS scaffolds may be used as a tool to alter cell functionality. GAG production, an indicator of chondrogenic potential,[62] was measured after culturing cells in chondrogenic media for 14 days. GAG production was significantly upregulated when cells were cultured on PEDOT-ACS, proving that the electroactive scaffold influences functionality and potentially differentiation. This scaffold may be an advantageous tool for proceeding investigations aimed towards understanding processes by which bioelectronic materials and electrical signals specifically drive chondrocyte differentiation or cartilage tissue engineering. The improvement in GAG production points to the importance of electromechanical influences in cartilage engineering, which are not currently well understood in the context of regeneration.

Conclusion

Here, we demonstrated an approach to integrate a collagen-based material with the CP, PEDOT-S. This technique effectively yielded a collagen composite with electroactive components that is mechanically comparable to the pristine collagen scaffold. Following incorporation, the zeta potential of the composite significantly decreased, attributable to the presence of negatively-charged PEDOT-S sulfonate groups. Additionally, the PEDOT-S composite enhanced cell viability, and a preliminary GAG production assay revealed the scaffold's promise to drive cells towards chondrogenesis.

Future work should be aimed at more in-depth investigations on the ability of electroactive materials such as PEDOT-S to drive cell phenomena and tissue repair. In the future, using a model system with a simpler architecture would allow for more elaborate studies on the mechanisms by which PEDOT-S complexes with dense protein structures and affects composite electroactivity. The approach described here incorporates CP into the scaffold only where there is an existing collagen structure, rather than through a method where PEDOT would form an independent percolative pathways as would be accomplished through in situ polymerization or other functionalization method. Because the ACS is a

highly porous, tortuous material, the PEDOT-S that templates onto it similarly has low percolation throughout, limiting the global conductivity of the PEDOT-ACS. The extent to which PEDOT-S enhances electronic and ionic conductivity of collagen could furthermore be better understood in the case of a simpler collagenous system. Additionally, more studies are warranted on the capability for electroactive materials to influence chondrogenesis specifically. Such studies would benefit by refining the approach presented here in a way that allows for variable material conductivity (i.e. polymer loading, chemical modification, etc.), without significantly impacting other important material properties, such as elastic modulus and macroscale architecture.

Acknowledgments

This work was primarily supported by an NSF ASCENT award (ECCS-2023849). RK was supported in part by the National Institutes of Health Training Grant (T32GM008449) through Northwestern University's Biotechnology Training Program. J.T. was primarily supported by an ONR YIP (SP0056955).

This work made use of the EPIC facility of Northwestern University's NUANCE Center, which has received support from the SHyNE Resource (NSF ECCS-2025633), the IIN, and Northwestern's MRSEC program (NSF DMR-1720139). This work made use of the DMA at the MatCI Facility supported by the MRSEC program of the National Science Foundation (DMR-1720139) at the Materials Research Center of Northwestern University. Zeta potential, absorbance, RT-qPCR measurements were performed in the Analytical bioNanoTechnology Core Facility of the Simpson Querrey Institute at Northwestern University. ANTEC is currently supported by the Soft and Hybrid Nanotechnology Experimental (SHyNE) Resource (NSF ECCS-2025633). Imaging work was performed at the Northwestern University Center for Advanced Microscopy generously supported by NCI CCSG P30 CA060553 awarded to the Robert H Lurie Comprehensive Cancer Center. This work made use of the GIANTFab core facility at Northwestern

University. GIANTFab is supported by the Institute for Sustainability and Energy at Northwestern and the Office of the Vice President for Research at Northwestern.

Ethical Approval

No human or animal studies were carried out by the authors for this article.

Conflict of Interest

Rebecca L. Keate, Joshua Tropp, Carlos Serna III, and Jonathan Rivnay declare that they have no conflict of interest.

Uncategorized References

1. Foulds, I. S., and A. T. Barker. Human skin battery potentials and their possible role in wound healing. British Journal of Dermatology. 109:515-522, 1983.

2. Fukada, E., and I. Yasuda. On the piezoelectric effect of bone. Journal of the Physical Society of Japan. 12:1158-1162, 1957.

3. McLaughlin, K. A., and M. Levin. Bioelectric signaling in regeneration: Mechanisms of ionic controls of growth and form. Developmental Biology. 433:177-189, 2018.

4. Persson, K. M., R. Karlsson, K. Svennersten, S. Löffler, E. W. H. Jager, A. Richter-Dahlfors, P. Konradsson, and M. Berggren. Electronic control of cell detachment using a self-doped conducting polymer. Advanced Materials. 23:4403-4408, 2011.

5. Li, Y., X. Li, R. Zhao, C. Wang, F. Qiu, B. Sun, H. Ji, J. Qiu, and C. Wang. Enhanced adhesion and proliferation of human umbilical vein endothelial cells on conductive pani-pcl fiber scaffold by electrical stimulation. Materials Science and Engineering: C. 72:106-112, 2017.

6. He, J., Y. Liang, M. Shi, and B. Guo. Anti-oxidant electroactive and antibacterial nanofibrous wound dressings based on poly(ε-caprolactone)/quaternized chitosan-graft-polyaniline for full-thickness skin wound healing. Chemical Engineering Journal. 385:123464, 2020.

7. Geng, K., J. Wang, P. Liu, X. Tian, H. Liu, X. Wang, C. Hu, and H. Yan. Electrical stimulation facilitates the angiogenesis of human umbilical vein endothelial cells through mapk/erk signaling pathway by stimulating fgf2 secretion. American journal of physiology. Cell physiology. 317:C277-c286, 2019.

8. Lu, Y., Y. Wang, J. Zhang, X. Hu, Z. Yang, Y. Guo, and Y. Wang. In-situ doping of a conductive hydrogel with low protein absorption and bacterial adhesion for electrical stimulation of chronic wounds. Acta Biomater. 89:217-226, 2019.

9. Leipzig, N. D., R. G. Wylie, H. Kim, and M. S. Shoichet. Differentiation of neural stem cells in three-dimensional growth factor-immobilized chitosan hydrogel scaffolds. Biomaterials. 32:57-64, 2011.

10. Liu, Z., L. Dong, L. Wang, X. Wang, K. Cheng, Z. Luo, and W. Weng. Mediation of cellular osteogenic differentiation through daily stimulation time based on polypyrrole planar electrodes. Scientific Reports. 7:17926, 2017.

11. Guex, A. G., J. L. Puetzer, A. Armgarth, E. Littmann, E. Stavrinidou, E. P. Giannelis, G. G. Malliaras, and M. M. Stevens. Highly porous scaffolds of pedot:Pss for bone tissue engineering. Acta Biomater. 62:91-101, 2017.

12. Petty, A. J., R. L. Keate, B. Jiang, G. A. Ameer, and J. Rivnay. Conducting polymers for tissue regeneration in vivo. Chemistry of Materials. 32:4095-4115, 2020.

13. Guo, B., and P. X. Ma. Conducting polymers for tissue engineering. Biomacromolecules. 19:1764-1782, 2018.

14. Balint, R., N. J. Cassidy, and S. H. Cartmell. Conductive polymers: Towards a smart biomaterial for tissue engineering. Acta Biomater. 10:2341-2353, 2014.

15. Nezakati, T., A. Seifalian, A. Tan, and A. M. Seifalian. Conductive polymers: Opportunities and challenges in biomedical applications. Chemical Reviews. 118:6766-6843, 2018.

16. Prasopthum, A., Z. Deng, I. M. Khan, Z. Yin, B. Guo, and J. Yang. Three dimensional printed degradable and conductive polymer scaffolds promote chondrogenic differentiation of chondroprogenitor cells. Biomaterials Science. 8:4287-4298, 2020.

17. Damaraju, S. M., Y. Shen, E. Elele, B. Khusid, A. Eshghinejad, J. Li, M. Jaffe, and T. L. Arinzeh. Three-dimensional piezoelectric fibrous scaffolds selectively promote mesenchymal stem cell differentiation. Biomaterials. 149:51-62, 2017.

18. Richardson, S. M., G. Kalamegam, P. N. Pushparaj, C. Matta, A. Memic, A. Khademhosseini, R. Mobasheri, F. L. Poletti, J. A. Hoyland, and A. Mobasheri. Mesenchymal stem cells in regenerative medicine: Focus on articular cartilage and intervertebral disc regeneration. Methods. 99:69-80, 2016.

19. Johnson, V. L., and D. J. Hunter. The epidemiology of osteoarthritis. Best practice & research. Clinical rheumatology. 28:5-15, 2014.

20. Hootman, J. M., C. G. Helmick, K. E. Barbour, K. A. Theis, and M. A. Boring. Updated projected prevalence of self-reported doctor-diagnosed arthritis and arthritis-attributable activity limitation among us adults, 2015-2040. Arthritis Rheumatol. 68:1582-1587, 2016.

21. Li, Y., X. Wei, J. Zhou, and L. Wei. The age-related changes in cartilage and osteoarthritis. BioMed research international. 2013:916530, 2013.

22. Bassett, C. A. L., and R. J. Pawluk. Electrical behavior of cartilage during loading. Science. 178:982, 1972.

23. Mow, V. C., and X. E. Guo. Mechano-electrochemical properties of articular cartilage: Their inhomogeneities and anisotropies. Annu. Rev. Biomed. Eng. 4:175-209, 2002.

24. Wang, C., T. Yokota, and T. Someya. Natural biopolymer-based biocompatible conductors for stretchable bioelectronics. Chemical Reviews. 121:2109-2146, 2021.

25. Irawan, V., T.-C. Sung, A. Higuchi, and T. Ikoma. Collagen scaffolds in cartilage tissue engineering and relevant approaches for future development. Tissue Engineering and Regenerative Medicine. 15:673-697, 2018.

26. Liu, X., C. Zheng, X. Luo, X. Wang, and H. Jiang. Recent advances of collagen-based biomaterials: Multi-hierarchical structure, modification and biomedical applications. Materials Science and Engineering: C. 99:1509-1522, 2019.

27. Ohyabu, Y., T. Adegawa, T. Yoshioka, T. Ikoma, K. Shinozaki, T. Uemura, and J. Tanaka. A collagen sponge incorporating a hydroxyapatite/chondroitinsulfate composite as a scaffold for cartilage tissue engineering. Journal of Biomaterials Science, Polymer Edition. 20:1861-1874, 2009.

28. Whitehouse, M. R., N. R. Howells, M. C. Parry, E. Austin, W. Kafienah, K. Brady, A. E. Goodship, J. D. Eldridge, A. W. Blom, and A. P. Hollander. Repair of torn avascular meniscal cartilage using undifferentiated autologous mesenchymal stem cells: From in vitro optimization to a first-in-human study. STEM CELLS Translational Medicine. 6:1237-1248, 2017.

29. Chen, G., and N. Kawazoe. Porous scaffolds for regeneration of cartilage, bone and osteochondral tissue. In: Osteochondral tissue engineering: Nanotechnology, scaffolding-related developments and translation. J. M. Oliveira, S. Pina, R. L. Reis and J. San Roman, eds. Springer International Publishing, Cham. pp 171-191, 2018.

30. Abedi, A., M. Hasanzadeh, and L. Tayebi. Conductive nanofibrous chitosan/pedot:Pss tissue engineering scaffolds. Materials Chemistry and Physics. 237:121882, 2019.

31. Sirivisoot, S., R. Pareta, and B. S. Harrison. Protocol and cell responses in three-dimensional conductive collagen gel scaffolds with conductive polymer nanofibres for tissue regeneration. Interface Focus. 4:20130050, 2014.

32. Dauzon, E., A. E. Mansour, M. R. Niazi, R. Munir, D.-M. Smilgies, X. Sallenave, C. Plesse, F. Goubard, and A. Amassian. Conducting and stretchable pedot:Pss electrodes: Role of additives on self-assembly, morphology, and transport. ACS Applied Materials & Interfaces. 11:17570-17582, 2019.

33. Donahue, M. J., A. Sanchez-Sanchez, S. Inal, J. Qu, R. M. Owens, D. Mecerreyes, G. G. Malliaras, and D. C. Martin. Tailoring pedot properties for applications in bioelectronics. Materials Science and Engineering: R: Reports. 140:100546, 2020.

34. Kayser, L. V., and D. J. Lipomi. Stretchable conductive polymers and composites based on pedot and pedot:Pss. Advanced Materials. 31:1806133, 2019.

35. Müller, C., M. Hamedi, R. Karlsson, R. Jansson, R. Marcilla, M. Hedhammar, and O. Inganäs. Woven electrochemical transistors on silk fibers. Advanced Materials. 23:898-901, 2011.

36. Karlsson, R. H., A. Herland, M. Hamedi, J. A. Wigenius, A. Åslund, X. Liu, M. Fahlman, O. Inganäs, and P. Konradsson. Iron-catalyzed polymerization of alkoxysulfonate-functionalized 3,4-ethylenedioxythiophene gives water-soluble poly(3,4-ethylenedioxythiophene) of high conductivity. Chemistry of Materials. 21:1815-1821, 2009.

37. Stéphan, O., P. Schottland, P.-Y. Le Gall, C. Chevrot, C. Mariet, and M. Carrier. Electrochemical behaviour of 3, 4-ethylenedioxythiophene functionalized by a sulphonate group. Application to the preparation of poly(3, 4-ethylenedioxythiophene) having permanent cation-exchange properties. Journal of Electroanalytical Chemistry. 443:217-226, 1998.

38. Beaumont, C., J. Turgeon, M. Idir, D. Neusser, R. Lapointe, S. Caron, W. Dupont, D. D'Astous, S. Shamsuddin, S. Hamza, É. Landry, S. Ludwigs, and M. Leclerc. Water-processable self-doped conducting polymers via direct (hetero)arylation polymerization. Macromolecules. 54:5464-5472, 2021.

39. Lutz, V., M. Sattler, S. Gallinat, H. Wenck, R. Poertner, and F. Fischer. Impact of collagen crosslinking on the second harmonic generation signal and the fluorescence lifetime of collagen autofluorescence. Skin Research and Technology. 18:168-179, 2012.

40. Ma, L., C. Gao, Z. Mao, J. Zhou, and J. Shen. Biodegradability and cell-mediated contraction of porous collagen scaffolds: The effect of lysine as a novel crosslinking bridge. Journal of Biomedical Materials Research Part A. 71A:334-342, 2004.

41. Nocera, A. D., R. Comín, N. A. Salvatierra, and M. P. Cid. Development of 3d printed fibrillar collagen scaffold for tissue engineering. Biomed. Microdevices. 20:26, 2018.

42. Rabbani, A., and S. Salehi. Dynamic modeling of the formation damage and mud cake deposition using filtration theories coupled with sem image processing. Journal of Natural Gas Science and Engineering. 42:157-168, 2017.

43. Ezeakacha, C. P., A. Rabbani, S. Salehi, and A. Ghalambor. Integrated image processing and computational techniques to characterize formation damage. In. 2018.

44. Yan, R., Y. Chen, Y. Gu, C. Tang, J. Huang, Y. Hu, Z. Zheng, J. Ran, B. Heng, X. Chen, Z. Yin, W. Chen, W. Shen, and H. Ouyang. A collagen-coated sponge silk scaffold for functional meniscus regeneration. Journal of tissue engineering and regenerative medicine. 13:156-173, 2019.

45. Sankoh, S., M. Y. Vagin, A. N. Sekretaryova, P. Thavarungkul, P. Kanatharana, and W. C. Mak. Colloid electrochemistry of conducting polymer: Towards potential-induced in-situ drug release. Electrochimica Acta. 228:407-412, 2017.

46. Itaka, K., S. Ohba, K. Miyata, H. Kawaguchi, K. Nakamura, T. Takato, U.-I. Chung, and K. Kataoka. Bone regeneration by regulated in vivo gene transfer using biocompatible polyplex nanomicelles. Molecular Therapy. 15:1655-1662, 2007.

47. Coulson-Thomas, V. J., and t. ferreira. Dimethylmethylene blue assay (dmmb). Bio-protocol. 4:e1236, 2014.

48. Zheng, C. H., and M. E. Levenston. Fact versus artifact: Avoiding erroneous estimates of sulfated glycosaminoglycan content using the dimethylmethylene blue colorimetric assay for tissue-engineered constructs. Eur Cell Mater. 29:224-236, 2015.

49. Beaumont, C., J. Turgeon, M. Idir, D. Neusser, R. Lapointe, S. Caron, W. Dupont, D. D'Astous, S. Shamsuddin, S. Hamza, É. Landry, S. Ludwigs, and M. Leclerc. Water-processable self-doped conducting polymers via direct (hetero)arylation polymerization. Macromolecules. 54:5464-5472, 2021.

50. Laura, M., C. David, I. M. Jean-Michel, and S. G. M. D. Warren. Characterization of type i, ii, iii, iv, and v collagens by time-resolved laser-induced fluorescence spectroscopy. In: Proc.SPIE. 2000.

51. Croce, A. C., and G. Bottiroli. Autofluorescence spectroscopy and imaging: A tool for biomedical research and diagnosis. Eur. J. Histochem. 58, 2014.

52. Shen, Y., D. Zhu, W. Lu, B. Liu, Y. Li, and S. Cao. The characteristics of intrinsic fluorescence of type i collagen influenced by collagenase i. Appl. Sci. 8:1947, 2018.

53. Tropp, J., M. H. Ihde, A. K. Williams, N. J. White, N. Eedugurala, N. C. Bell, J. D. Azoulay, and M. Bonizzoni. A sensor array for the discrimination of polycyclic aromatic hydrocarbons using conjugated polymers and the inner filter effect. Chem. Sci. 10:10247-10255, 2019.

54. Li, Y., A. Asadi, M. R. Monroe, and E. P. Douglas. Ph effects on collagen fibrillogenesis in vitro: Electrostatic interactions and phosphate binding. Materials Science and Engineering: C. 29:1643-1649, 2009.

55. Hamedi, M., A. Elfwing, R. Gabrielsson, and O. Inganäs. Electronic polymers and DNA self-assembled in nanowire transistors. Small. 9:363-368, 2013.

56. Hamedi, M., A. Herland, R. H. Karlsson, and O. Inganäs. Electrochemical devices made from conducting nanowire networks self-assembled from amyloid fibrils and alkoxysulfonate pedot. Nano Letters. 8:1736-1740, 2008.

57. Xiao, Y., C. M. Li, S. Wang, J. Shi, and C. P. Ooi. Incorporation of collagen in poly(3,4-ethylenedioxythiophene) for a bifunctional film with high bio- and electrochemical activity. Journal of Biomedical Materials Research Part A. 92A:766-772, 2010.

58. Sorushanova, A., L. M. Delgado, Z. Wu, N. Shologu, A. Kshirsagar, R. Raghunath, A. M. Mullen, Y. Bayon, A. Pandit, M. Raghunath, and D. I. Zeugolis. The collagen suprafamily: From biosynthesis to advanced biomaterial development. Advanced Materials. 31:1801651, 2019.

59. Müller, D., R. Cercená, A. J. Gutiérrez Aguayo, L. M. Porto, C. R. Rambo, and G. M. O. Barra. Flexible pedot-nanocellulose composites produced by in situ oxidative polymerization for passive components in frequency filters. Journal of Materials Science: Materials in Electronics. 27:8062-8067, 2016.

60. Zamora-Sequeira, R., I. Ardao, R. Starbird, and C. A. García-González. Conductive nanostructured materials based on poly-(3,4-ethylenedioxythiophene) (pedot) and starch/κ-carrageenan for biomedical applications. Carbohydrate Polymers. 189:304-312, 2018.

61. Wang, S., S. Guan, Z. Zhu, W. Li, T. Liu, and X. Ma. Hyaluronic acid doped-poly(3,4-ethylenedioxythiophene)/chitosan/gelatin (pedot-ha/cs/gel) porous conductive scaffold for nerve regeneration. Materials Science and Engineering: C. 71:308-316, 2017.

62. Barry, F., R. E. Boynton, B. Liu, and J. M. Murphy. Chondrogenic differentiation of mesenchymal stem cells from bone marrow: Differentiation-dependent gene expression of matrix components. Experimental Cell Research. 268:189-200, 2001.

Figure Legends

Figure 1. Scheme for Generation of CP-Collagen Composites (a) The facile approach described for adding the CP PEDOT-S to collagen matrices is shown here. **(b-c)** The ACS (left) demonstrates a visible color change, which can be attributed to the presence of PEDOT-S in the collagen matrix (right).

Figure 2. PEDOT-ACS Maintains Collagen Molecular Integrity, Macrostructure (a-b) Confocal imaging in the absence of added dyes demonstrate collagen sustained autofluorescence following the incorporation of PEDOT-S into the scaffold matrix. SEM micrographs **(c-d)** show that PEDOT-ACS

maintains qualitatively similar macrostructure based on the pore and sheet geometry of the scaffold structure compared to ACS control. Higher magnification SEMs **(e-f)** show the microstructure of these scaffolds qualitatively maintains fibrous structures in both ACS and PEDOT-ACS. Differences in porous microstructure of these scaffolds were quantified by measuring **(g)** scaffold volume porosity (n=3) **(p=0.04)** and **(h)** the distribution of pore radius for pores with radii up to 25 μm.

Figure 3. Influence of PEDOT-ACS on Collagen Structure (a) Compression testing (n=5) of PEDOT-ACS that had been cut into 10-mm discs revealed that materials have a significantly higher elastic modulus (16.40 ± 4.08 kPa) when dry compared to ACS (7.15 ± 1.70 kPa) **(p=0.001). (b)** Wet compression testing, however, revealed that PEDOT-ACS has a comparable modulus to the ACS (0.518 ± 0.161 kPa; 0.529 ± 0.020 kPa) **(p=0.88). (c)** Swelling properties of the scaffolds was analyzed after incubating scaffolds in DPBS for 2 days (n = 5). The sponge with PEDOT-S demonstrated a reduced swelling ratio (337.7 ± 14.6) compared to the ACS alone (361.5 ± 25.0) **(p=0.02).**

Figure 4. PEDOT-S Decreases Scaffold Surface Charge Zetasizer analysis, performed in triplicates on a single solution of scaffold particulates resuspended in 0.01 M NaCl, showed that PEDOT-ACS scaffolds had significantly lower surface charge (-19.9 ± 1.2 mV) compared to ACS (-9.9± 1.3 mV) **(p=0.0005).**

Figure 5. PEDOT-ACS Promotes Cell Viability Live/dead assays were performed with rBMSCs seeded on **(a)** ACS and **(b)** PEDOT-ACS. Cells on PEDOT-ACS were more elongated than the cells observed on ACS. **(c)** An alamarBlue cell health assay suggested that the PEDOT-S did not cause cytotoxicity. Measurements were performed to quantify cell health on days 0, 1, 2, 3, 5, and 7 (n=3) **(p=0.02, 0.11, 0.001, 0.006, 0.08, and 0.012).**

Figure 6. PEDOT-ACS Demonstrates Chondrogenic Potential A DMMB assay (n=3) was performed with rBMSCs cultured in chondrogenic media to measure cell GAG production, as an indicator of the potential

for PEDOT-ACS to induce chondrocyte differentiation. PEDOT-ACS demonstrated significantly higher GAG production per DNA content (1.1 ± 0.2) compared to ACS (0.4 ± 0.2) **(p=0.01).**

Figures

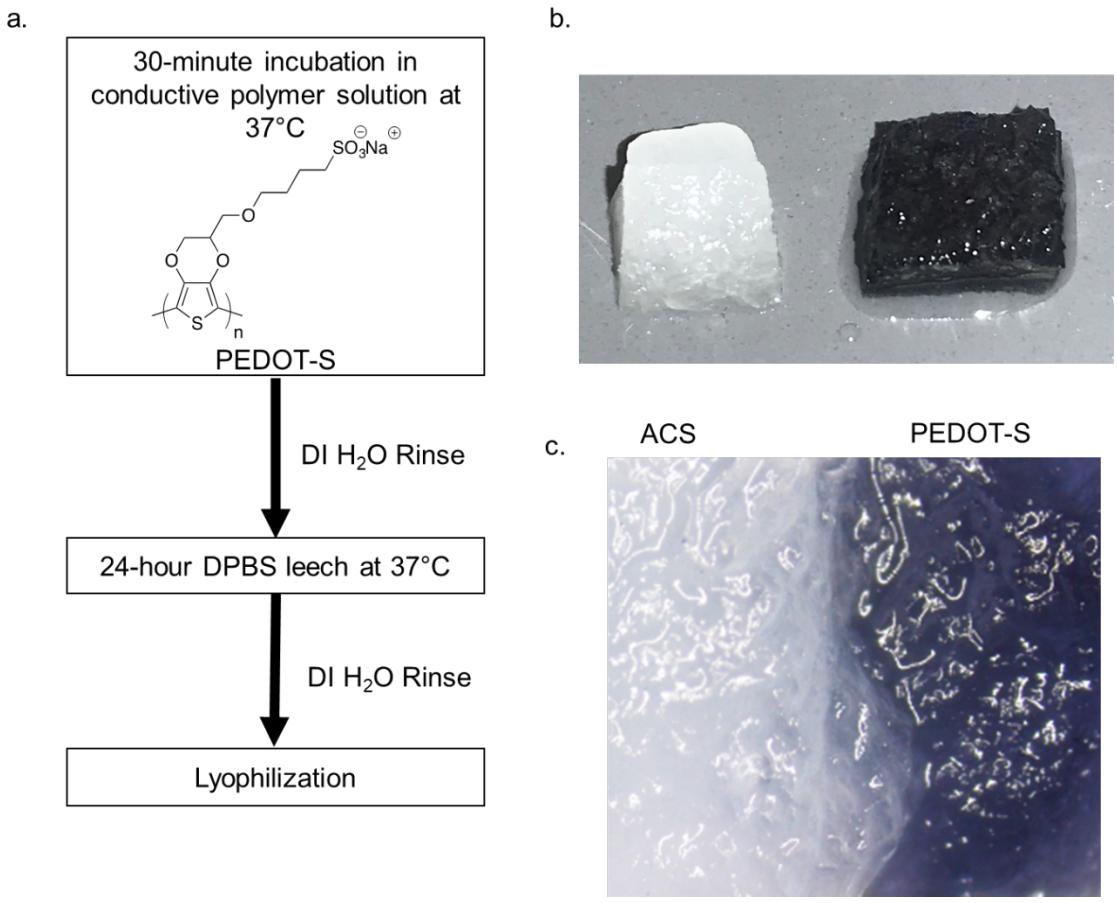

Figure 1, Rebecca L. Keate

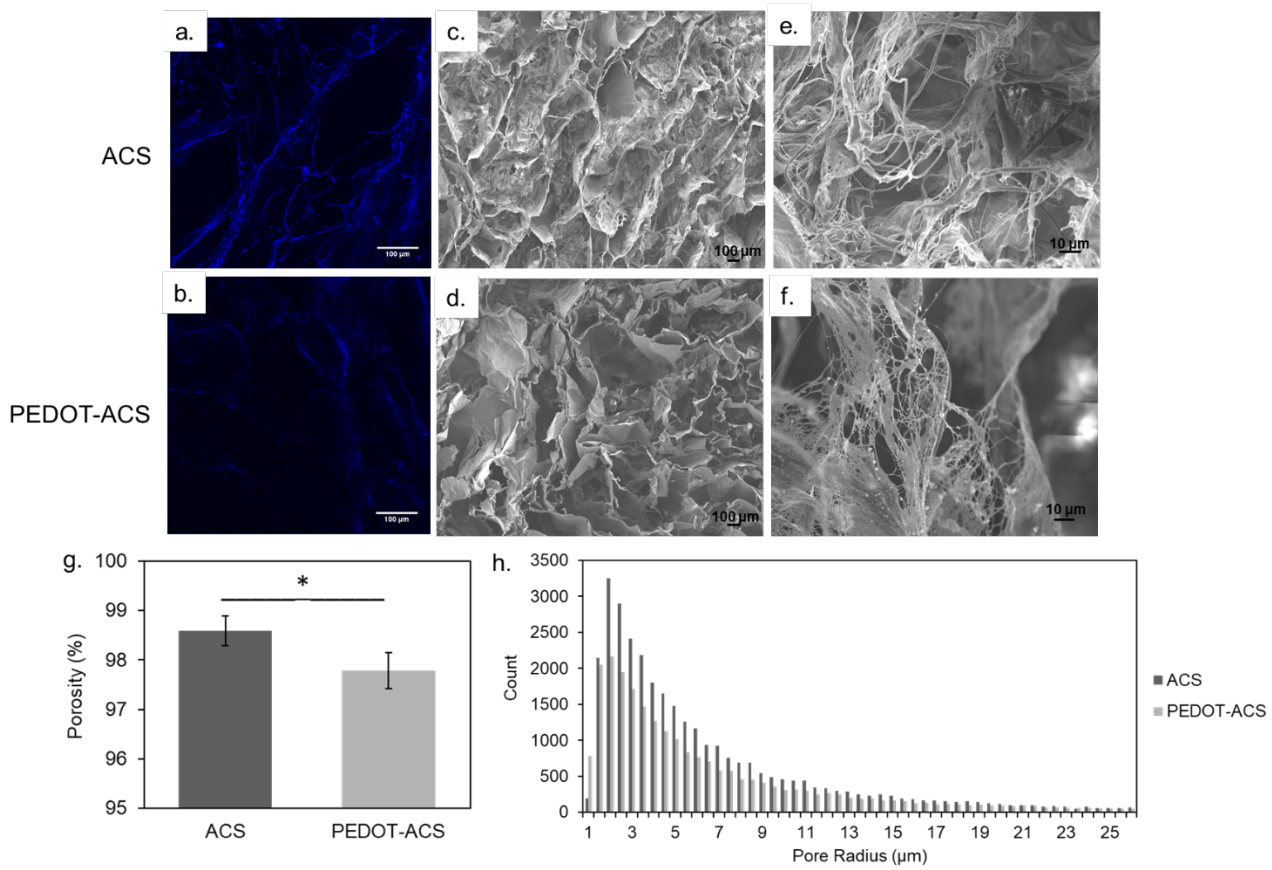

Figure 2, Rebecca L. Keate

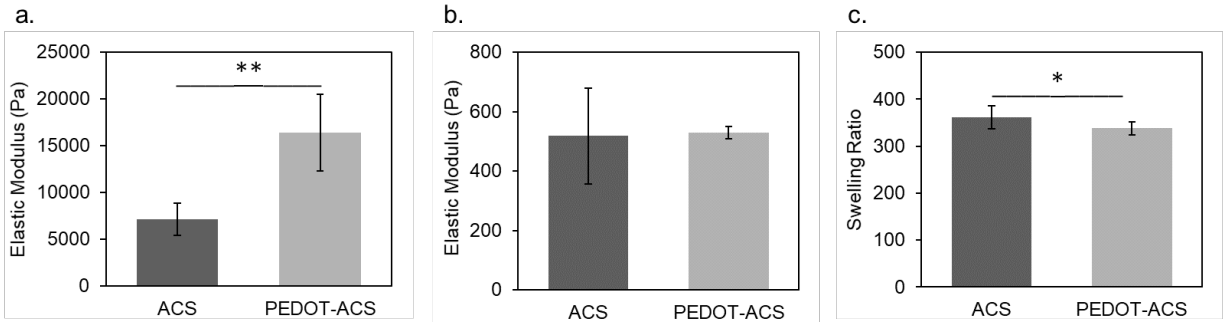

Figure 3, Rebecca L. Keate

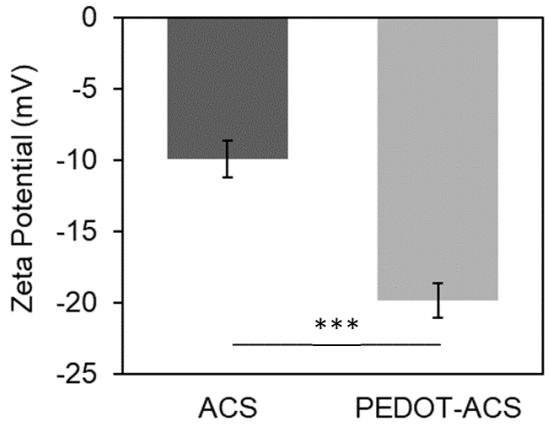

Figure 4, Rebecca L. Keate

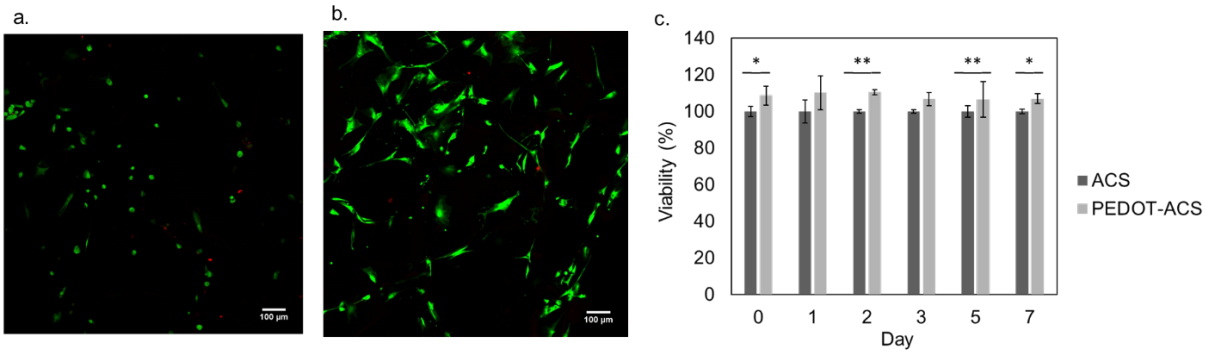

Figure 5, Rebecca L. Keate

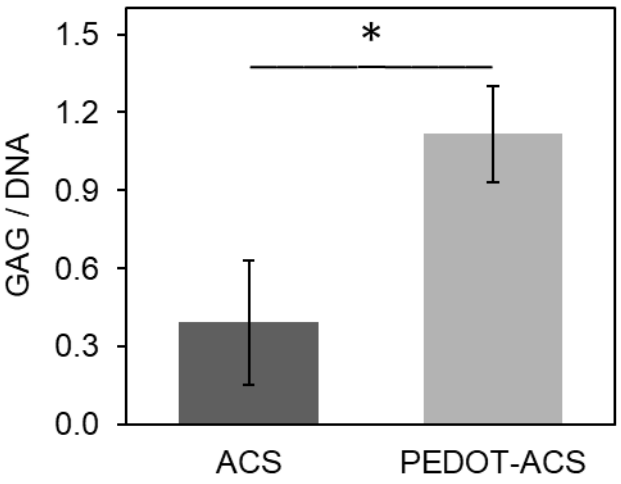

Figure 6, Rebecca L. Keate